Optical vortex coronagraphs on ground-based telescopes

Charles Jenkins
Research School of Astronomy and Astrophysics,
Australian National University, Cotter Road, Weston, ACT 2611,
Australia
charles.jenkins@anu.edu.au

February 1, 2008

Abstract

The optical vortex coronagraph is potentially a remarkably effective device, at least for an ideal unobstructed telescope. Most ground-based telescopes however suffer from central obscuration and also have to operate through the aberrations of the turbulent atmosphere. This note analyzes the performance of the optical vortex in these circumstances and compares to some other designs, showing that it performs similarly in this situation. There is a large class of coronagraphs of this general type, and choosing between them in particular applications depends on details of performance at small off-axis distances and uniformity of response in the focal plane. Issues of manufacturability to the necessary tolerances are also likely to be important.

1 Introduction

Many areas of astrophysics need a coronagraph of very high dynamic range, to detect faint sources near bright ones. Examples include exoplanets, protoplanetary disks, and the structure of active galactic nuclei. These applications cover a wide range of acceptable dynamic range, with planets being the most challenging.

A wide variety of coronagraphs has been proposed[1] and one particularly impressive one is the optical vortex coronagraph (OVC). This a remarkable example of diffraction at work [2, 3, 4]. A "vortex phase mask" (VPM) is introduced at the focus at the focus of a circularly symmetric optical system. In the best-studied examples, this mask introduces a phase proportional to $m\theta$, where θ is an azimuthal co-ordinate in the focal plane, and m is an even integer called the topological charge. If the diffraction pattern at the focus is an Airy function, then one finds exactly, i.e. analytically, that all of the light in this diffraction pattern is diffracted outside the re-imaged pupil. A simple Lyot stop will thus extinguish all of the light from an on-axis source, at least for perfect optics. Actual implementations of a VPM will have imperfections, including possibly a loss of amplitude close to the vortex core, depending on how the VPM is implemented. Here I concentrate on an ideal system.

The vortex phase mask appears to form the basis of a very elegant coronagraph. It has high performance by comparison with other designs [5], and can be designed to be achromatic [6] and insensitive to aberrations. [7] Its conception can be seen as a continuation of related designs – the phase-mask coronagraph [8] and the four-quadrant phase-mask coronagraph. [9]

It is of interest to examine the performance of the OVC on ground-based telescopes. These generally have two features which are not favourable for the OVC - a central obstruction, and images blurred by atmospheric turbulence. I will examine both aspects and show that the OVC behaves similarly to some other designs, but with good performance and some advantages even in these non-ideal circumstances.

The non-ideal PSF – the central obstruction

For any coronagraph, the loss of Strehl ratio from a central obstruction is a disadvantage. The OVC is no exception; in the reimaged pupil, the secondary is surrounded by a halo of light, whose total power is comparable to the power obstructed by the secondary. This result is illustrated by direct computation in Figure 1.

This result can be examined analytically, as is discussed elsewhere in detail by Mawet *et al.*[10]. Only the central obstruction need be added to their comprehensive treatment. I discuss a mask of charge 2 as an example. Using standard Fraunhofer diffraction, the amplitude, in a reimaged pupil plane beyond the VPM, is given by a generalized Hankel transform:

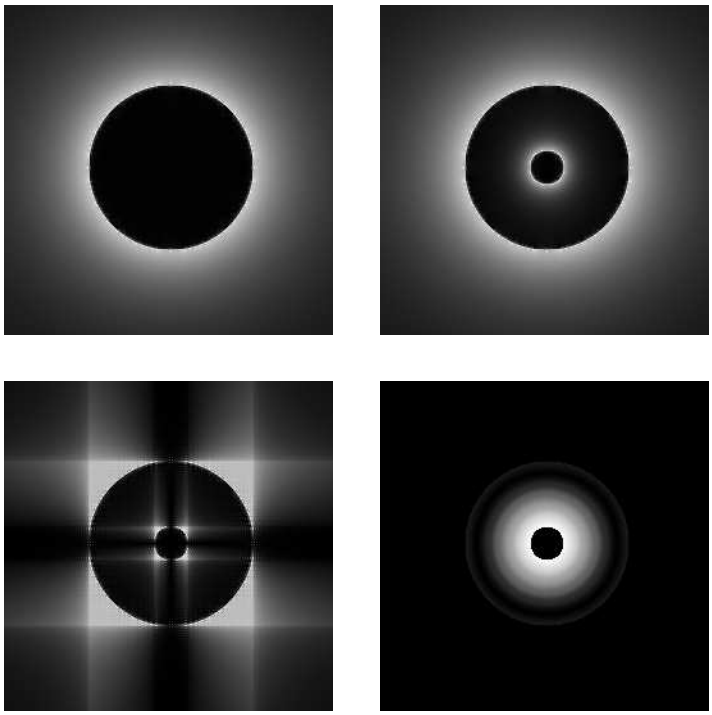

Figure 1: The intensity pattern in the reimaged pupil plane beyond a VPM, for an obstructed and unobstructed pupil. This was computed by direct FFT for perfect optics and charge 2 (top left), for charge 2 with a central obstruction (top right), for a quadrant phase mask (bottom left) and an optimum prolate apodization (bottom right).

$$\mathcal{A}(r') = Ke^{2\imath\beta} \int_0^\infty \mathcal{F}(k)\, J_2(kr')k\, dk$$

in which r and k are suitably scaled radial co-ordinates in the reimaged pupil and the preceding focal plane, and β is an azimuthal angle in the reimaged pupil. Constants irrelevant to the discussion are absorbed into K. $\mathcal{F}$ is the amplitude in the focal plane for an on-axis source. If this is an Airy function for an input pupil of radius R, the integral becomes

$$\mathcal{A}(r) = Ke^{2\imath\beta} R \int_0^\infty J_1(kR)\, J_2(kr')\, dk.$$

(The second-order Bessel function arises because the amplitude introduced by the VPM has been taken to be $e^{2\imath\theta}$ in this example. This topological charge of 2, via the angular integral of the Fourier transform, translates directly into the order of the Bessel function. The needed result is

$$\int_0^{2\pi} e^{2\imath\theta} e^{\imath k(\theta-\beta)}\, d\theta = -2\pi e^{2\imath\beta} J_2(k)\,)$$

(see equation 5).

The infinite integral is a case of the Weber-Schafheitlin integral [11], and so

$$\begin{aligned} \mathcal{A}(r') &= 0 && 0 \le r' < R \\ &= K e^{2\imath\beta} (\tfrac{R}{r'})^2 && r' \ge R \end{aligned} \tag{1}$$

for the amplitude in the reimaged pupil. This is the result that motivates the optical vortex coronagraph; similar results can be obtained for other even topological charges of the VPM. The power diffracted outside R is $|K|^2\pi R^2$, which is exactly equal to the power in the focal plane diffraction pattern $(J_1(kR)/kR)^2$. In the case of a centrally obstructed pupil, however, an on-axis source at infinity produces an amplitude in the focal plane that is given by

$$\mathcal{F}(k) = K(\frac{RJ_1(kR)}{k} - \frac{aJ_1(ka)}{k})$$

in which a is the radius of the central obstruction. It follows that the amplitude in the reimaged pupil must be

$$\begin{aligned} \mathcal{A}(r') &= 0 && 0 \le r' < a \\ &= -K e^{2\imath\beta} (\tfrac{a}{r'})^2 && a \ge r' < R \\ &= K e^{2\imath\beta} \left((\tfrac{R}{r'})^2 - (\tfrac{a}{r'})^2 \right) && R \ge r' \end{aligned} \tag{2}$$

The total diffracted power is now $|K|^2\pi(R^2-a^2)$, and the power diffracted into the reimaged pupil between a and R is $|K|^2\pi a^2(1-(a/R)^2)$. The total energy diffracted into the halo of the secondary is nearly equal to the energy incident upon it, particularly for typical telescopes where a is much less than R.

A first-order approach to evaluating this issue is simply to examine the total power which passes through a Lyot stop. In fact, one might also consider blocking some of the diffracted light with an enlarged stop at the secondary; while this costs light, it might yield a net benefit in terms of attainable dynamic range.

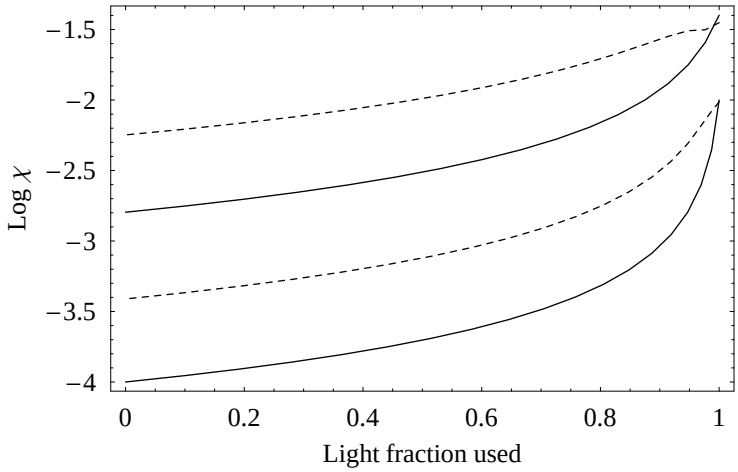

Figure 2: The normalized diffracted power χ, plotted against the fraction of the light that is admitted through a centrally-obstructed Lyot stop. The curves are for linear central obstructions a/R of 0.2 and 0.1. The full line is for a VPM of charge 2, the dashed line for charge 4.

Using Equation 2, the fraction of the power from an on-axis source that appears between $\rho > a$ and R is

$$\begin{aligned} \chi &= \left(\int \left(\frac{a}{r} \right)^4 2\pi r \, dr \right) / \left(\pi (R^2 - \rho^2) \right) \\ &= \frac{a^4}{R^2 \rho^2}. \end{aligned} \tag{3}$$

This is the fraction of the energy of the the on-axis source that passes the proposed Lyot stop. This may usefully be compared to the fraction of the available light that is used in this scheme, which is

$$\frac{R^2 - \rho^2}{R^2 - a^2}$$

as is shown in Figure 2. For modest loss of light ($\sim$ 20%) the attainable dynamic range is about 100; this may be useful, especially if the dynamic range is more fundamentally limited by adaptive optics considerations. Losing light is not always a disaster if another parameter is improved, in this case dynamic range, but it is clear that the sacrifice would have to be very substantial to attain high dynamic range.

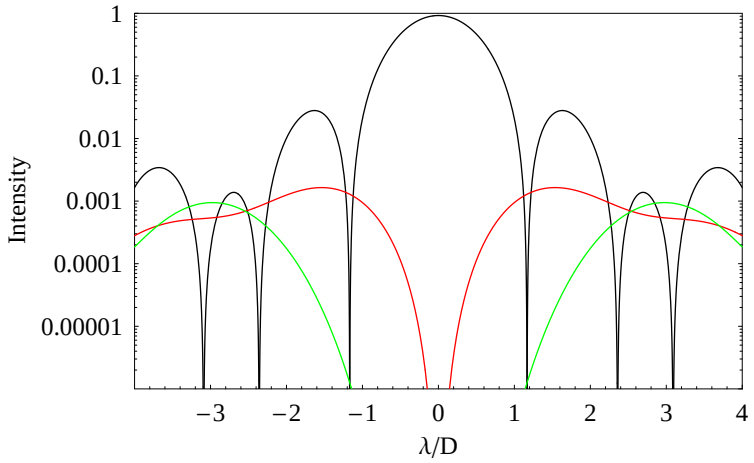

Figure 3: Calculations of the final point-spread function, for an on-axis object. The intensities are normalized to the diffraction-limited case with no central obstruction. Colours code the no-vortex case $m = 0$ (black), charge 2 (red), and $m = 6$ (green), all with a 20% linear central obstruction.

A fuller evaluation looks at the point-spread function of an on-axis source, imaged through the VPM and a standard Lyot stop. This involves a Hankel transform of the amplitude in $a \geq r' < R$, as given by Equation 2 (or its extension for higher charges than 2). This integral is again of the Weber-Schafheitlin form. For charge 2, for example, the final focal-plane amplitude, in terms of a radial co-ordinate k', is proportional to

$$a^2 \left(\frac{J_1(k'a)}{k'a} - \frac{J_1(k'R)}{k'R} \right).$$

Examples of the PSFs are shown in Figure 3, where it is seen that the effects of the central obstruction are felt in different parts of the image, depending on the charge on the VPM. Depending on application, this level of light pollution may be acceptable.

For a ground-based telescope, partial correction for atmospheric turbulence may be a more relevant limitation to consider. Anticipating the discussion of Section 2, Figure 4 shows that the effect of a central obstruction could be quite perceptible. In this example the available "dark" region is completely filled by diffracted light.

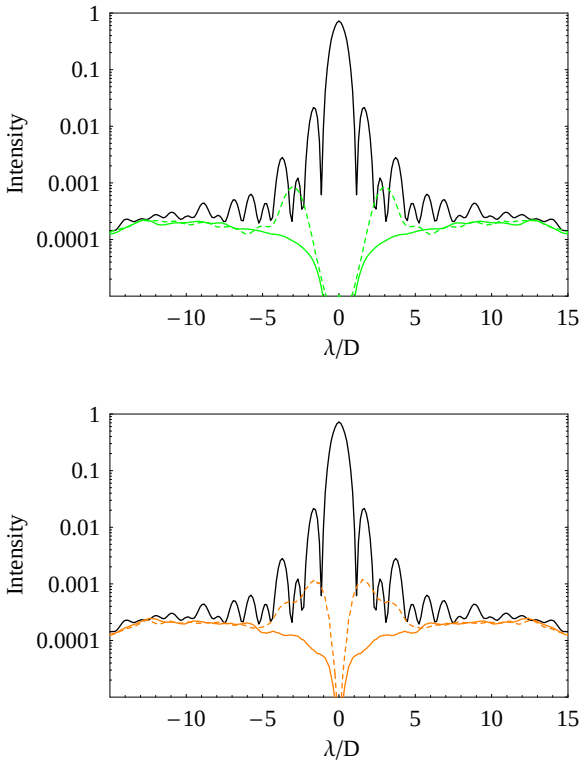

Figure 4: Simulation results, described later, for the on-axis long-exposure point spread function in a well-corrected AO case. The intensities are normalized to the diffraction-limited case. Colours code the no-vortex case $m = 0$ (black), charge 6 VPM (solid green), and a quadrant phase mask (solid orange). Dashed lines are for a case with a 20% linear central obstruction.

Several methods are possible to recover the performance of the vortex coronagraph. For example, one might use a focal plane occulting stop as a second stage. Because the images formed on-axis through a VPM are quite wide (Figure 4) this stop would have to be large.

Another option is to eliminate the central obstruction of the telescope, perhaps by using an off-axis Herschel-like system[12], as is proposed for the Terrestrial Planet Finder mission. Large off-axis paraboloids are now being manufactured for the Giant Magellan Telescope [13], which will contain six adjacent mirrors in an outer ring. From the Fourier shift theorem, the amplitudes in the reimaged pupils will simply be displaced versions of Equation 1, so that the issue will become the light pollution between mirrors (Figure 5). By using some subset of the available mirrors in a dilute aperture configuration, light pollution may be substantially reduced, although at the cost of losing light-gathering power. This is an example of how the central-obstruction problem may be handled with a more dilute aperture. Detailed calculation would be necessary to establish that the light pollution was acceptable for a particular configuration of apertures. An additional option would be to include stops close to the focal plane that prevented light pollution from one aperture to the other, although this would limit field of view.

The most attractive approach seems to be Guyon's [14] technique of phase-induced amplitude apodization. This reshapes the illumination of the pupil, using the complex aspheric surfaces which it is now possible to manufacture. Guyon gives examples in which the central obstruction os a two-mirror telescope is eliminated completely. Guyon was also concerned to tailor the resulting point-spread function so that it had low sidelobes, but there seems no reason why his technique should not be used in a simpler way to produce a pure Airy disk for an on-axis source. Apart from manufacturability, which is still costly, the main limitation to the method is the narrow field of view. If the pupil were reshaped to eliminate the central obstruction, then an off-axis source will have a phase discontinuity at the centre of the reshaped pupil. This will limit the field to an angular extent given by the diffraction limit of a pupil of equal size to the obstruction. This will probably not be a limitation however in the very narrow-field applications of high-contrast coronography. It is also possible to avoid this field-of-view limitation by a second stage of pupil reshaping after the VPM, in which the original pupil is restored.[14]

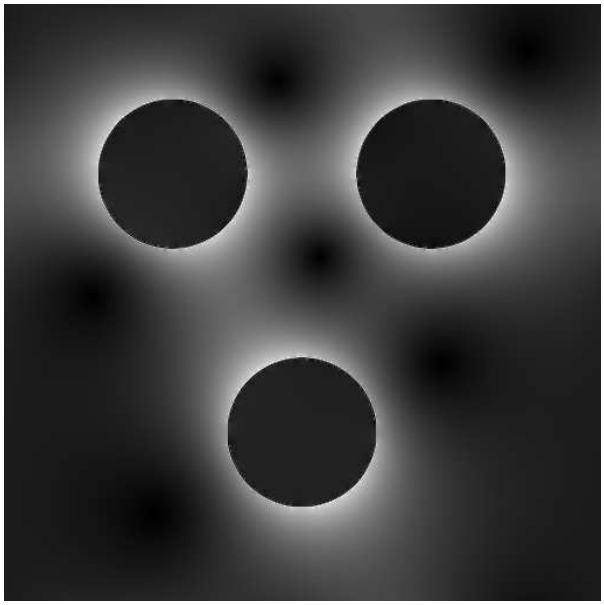

Figure 5: The intensity pattern in the reimaged pupil plane beyond a VPM, for an illustrative telescope containing three off-axis mirrors.

2 The non-ideal PSF – partial AO correction

A coronagraph on a ground-based telescope will probably be designed to deal with a partially-corrected image, where the effects of atmospheric turbulence have been partially removed. Such designs have been made, for example, for the VLT [15, 16] and Gemini [17] telescopes.

In what follows I will assume that the central obstruction either does not exist or has been removed by Guyon's method. As Figure 4 shows, this is important.

The Point Spread Function (PSF) of an adaptive optics system is of course affected by a large number of parameters, but when residual phase errors are small the PSF is well approximated by a diffraction-limited core, flanked by a halo whose functional form is given by the power spectrum of the residual phase. An optimized AO system can largely remove low spatial frequencies from the atmospheric phase power spectrum, but scales within or comparable to actuator spacings cannot be removed. The overall effect is that the diffraction-limited part of the PSF sits in a "hole" in the power-law

halo.

Some analytical progress is possible in the case of well-corrected images, and this provides a valuable guide to what may be expected and a check in various cases of numerical simulations. This is useful in coronagraphic applications where a large dynamic range is enquired in the calculation and small numerical errors may become relatively important. The essential results are the effect of a PVM on a partially-corrected image, and some knowledge of the throughput of these systems for targets that are not quite on-axis (the targets of interest of course).

It is possible to calculate the form of the PSF in the limiting case of good correction with high actuator density, for a coronagraph built around a VPM. The calculation is outlined in Appendix 1, and shows that the coherent diffraction-limited core is simply removed from the PSF, with only the halo (the residual phase power spectrum) remaining. This is intuitively what one would expect, since the VPM is fundamentally an interference device.

In Appendix 2 it is shown that the throughput of a OVC, for an off-axis source, is a strong power-law function of offset distance, with the index depending on the charge of the mask.

Finally, in Appendix 3 it is shown that a wide variety of useful phase masks are, in effect, superpositions of VPMs.

Taken together, these results suggest that the attainable dynamic range of OVCs and related systems, in the partially-corrected AO case, will converge at large radii to values fixed by the AO system itself, while more marked variations in performance will be apparent at small radii. To investigate this in more detail, three general-purpose coronagraphic designs will be studied: OVCs for charges 2 and 6, a quadrant phase mask [9], and a prolate-apodized mask [18]. The prolate mask affects amplitude, not phase, and so gives excellent performance at the expense of a loss of light. The example used here is the $\Lambda = 0.99$ case reported by Soummer et al., which transmits only 26% of the incident energy.

Calculating the performance of these systems in the case of partial AO correction requires Monte Carlo simulation. The technique used here for numerical simulations is discussed in detail by Sivaramakrishnan *et al.*.[19]. These authors describe a useful way of summarizing the AO system performance with just two parameters, the initial uncorrected turbulence strength (the usual D/r_0) and an effective actuator spacing $d_{\rm eff}$. Two illustrative AO systems are modelled here to investigate the performance of the OVC. The first is a fairly high-performance AO system, with $D/r_0 = 10$ and

$D/d_{\text{eff}} = 25$. Here the diffraction-limited part of the PSF is quite large (extending to about $8\lambda/D$. The second models a more general-purpose AO system, with $D/r_0 = 10$ and $D/d_{\text{eff}} = 10$.

Some care has to be taken in these numerical simulations as very large arrays would be needed both to eliminate low-level aliasing effects and also to give adequate detail in the computed PSFs. For the results to be discussed, an aperture of 128 pixels diameter was embedded in a 1024 square array. The results were checked explicitly against analytical results, both the absolute accuracy and for trends.

Aliasing is an issue for the high levels of accuracy that are required in this type of simulation. The VPM diffracts light symmetrically outside the pupil according to a power law, and this slow decline aliases back into the pupil where there should be zero amplitude. The effect is small but perceptible. It can be largely eliminated by deriving the amplitude within the pupil for a diffraction-limited source, and then subtracting this from calculations in other cases. One check on this method is to compare analytical solutions for an obstructed telescope with the simulations corrected in this way (see Figure 6) - the method works well for the VPMs, giving reliable results at the 10^6 level of dynamic range. The quadrant mask simulations work well to at least this level without any corrections, probably because of the strong angular modulation of extra-pupil diffracted light (Figure 1).

The results are shown in Figures 7 and 8. The diffraction-limited "core" region is apparent, transitioning into the power-law "halo". The halo is unaffected by the coronagraphs and the interesting region is within the "shoulder" that marks the transition. The extent of this region is determined by the turbulence strength and the actuator density.

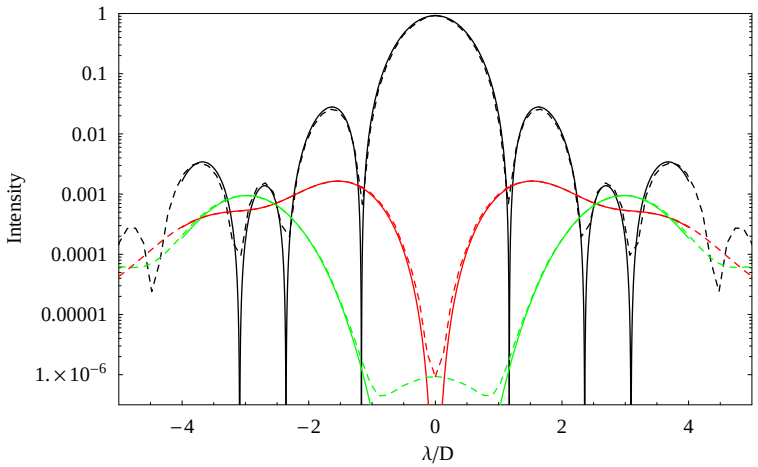

Figure 6: A comparison of analytical results for the PSF with numerical calculations for a diffraction-limited telescope with a 20% linear central obstruction. Colours code the no-vortex case $m = 0$ (black), charges 2 (red) and 6 (green). Dashed lines are for the numerical calculations, which are for a 128-pixel diameter aperture embedded in a 1024-pixel square array, with an aliasing correction as described in the text.

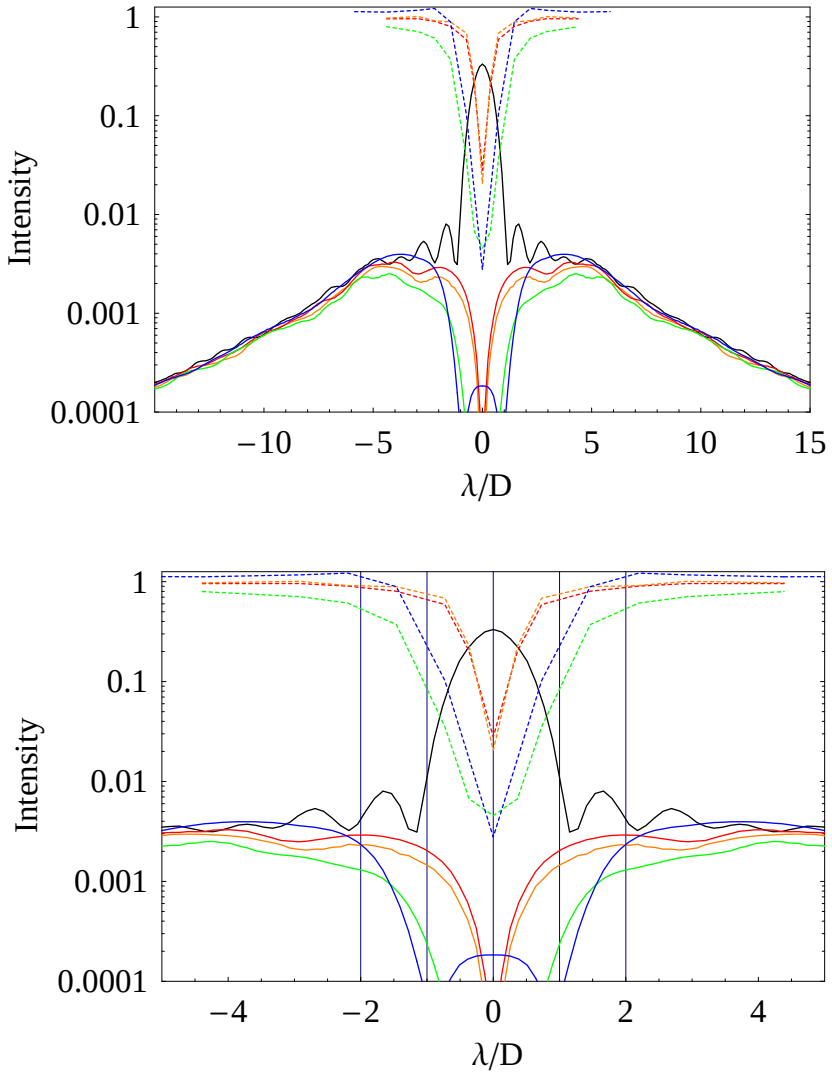

Figure 7: Simulation results for the long-exposure point spread function of an on-axis source, for a the modestly-corrected AO case (no central obstruction, $d_{\rm eff} = r_0$). The intensities are normalized to the diffraction-limited case. Colours code the no-vortex case $m = 0$ (black), charges 2 (red) and 6 (green), as well as the quadrant phase mask (orange) and prolate-apodized mask (blue). Dashed lines show the relative throughput for an off-axis source, as a function of off-axis distance. Calculations for the quadrant phase mask, here and elsewhere, were at the optimum 45° to the lines of phase discontinuity.

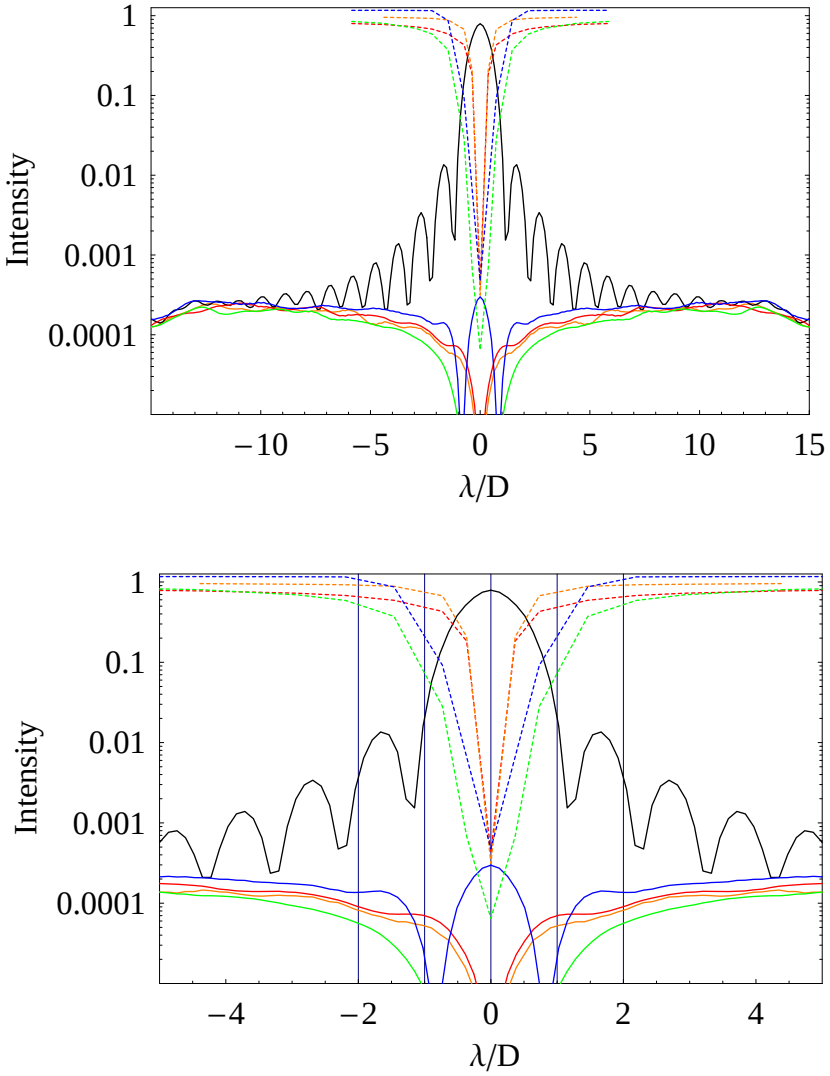

Figure 8: Simulation results for the long-exposure point spread function of an on-axis source, for a well-corrected AO case (no central obstruction, $2.5d_{\rm eff} = r_0$). The intensities are normalized to the diffraction-limited case. Colours code the no-vortex case $m = 0$ (black), charges 2 (red) and 6 (green), as well as the quadrant phase mask (orange) and prolate-apodized mask (blue). Dashed lines show the relative throughput for an off-axis source, as a function of off-axis distance.

Each coronagraphic method works similarly outside a few λ/D. As expected, the coherent core of the PSF is largely removed, and so the attainable dynamic range is simply set by the strength of the PSF halo at the shoulder. There are strong differences in effectiveness within $\sim 2\lambda/D$. These are ambitiously small offsets to consider, since aberrations and scattering in the telescope are extremely difficult to control at these levels. Nonetheless, the ultimate purpose of coronagraphs is to be effective at a few λ/D.

The question then arises of how well the various coronagraphs would transmit an off-axis source. What is the exclusion radius r_c beyond which a source is unaffected by the coronagraph?

In the case of the OVC r_c can be estimated by requiring that the phase introduced by the OVC (charge m), across the off-axis source, should be less than about π. Hence

$$r_c = \frac{m}{\pi}\frac{\lambda}{D}$$

suggesting that high-charge OVCs will not be able to detect companion sources as close as low-charge ones. In fact, it is possible to calculate analytically the response of an OVC to off-axis sources in the diffraction limit (see Appendix 2) and this shows that, close to on-axis, the response is a very strong function of charge. Larger charges attenuate very strongly close to the axis. Combining these two results suggests that overall higher charges should have bigger exclusion radii and is a useful analytical verification of the trends in the simulation results.

For the quadrant mask a narrow radius of exclusion is expected, roughly $r_c = (2/\pi)(\lambda/D)$ and rather like a charge 2 OVC. The prolate case is too complicated to estimate because of diffraction at a stop in the focal plane.

As a source emerges "from the vortex" the PSF is quite distorted (Figure 9). To quantify the exclusion radius I used as a metric the flux through a small circular aperture, extending out to the first (diffraction limited) dark ring and centered at the input position of the off-axis test source. This is normalized to the flux through the same aperture for the partially-corrected PSF, with no coronagraph. The results for the four coronagraphs are superimposed on Figures 7 and 8.

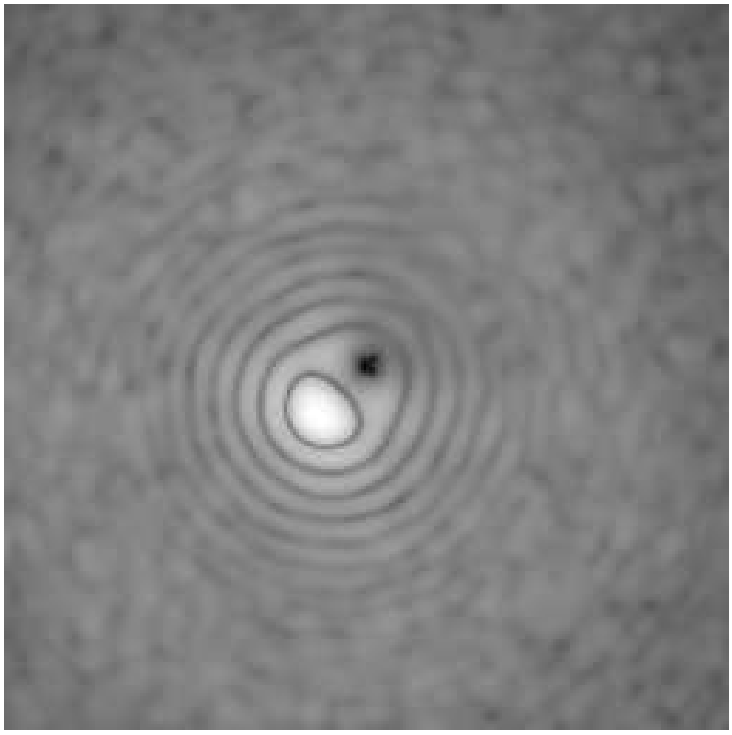

Figure 9: A gray-scale image illustrating a source emerging from the vortex in the $m = 6$ well=corrected case.

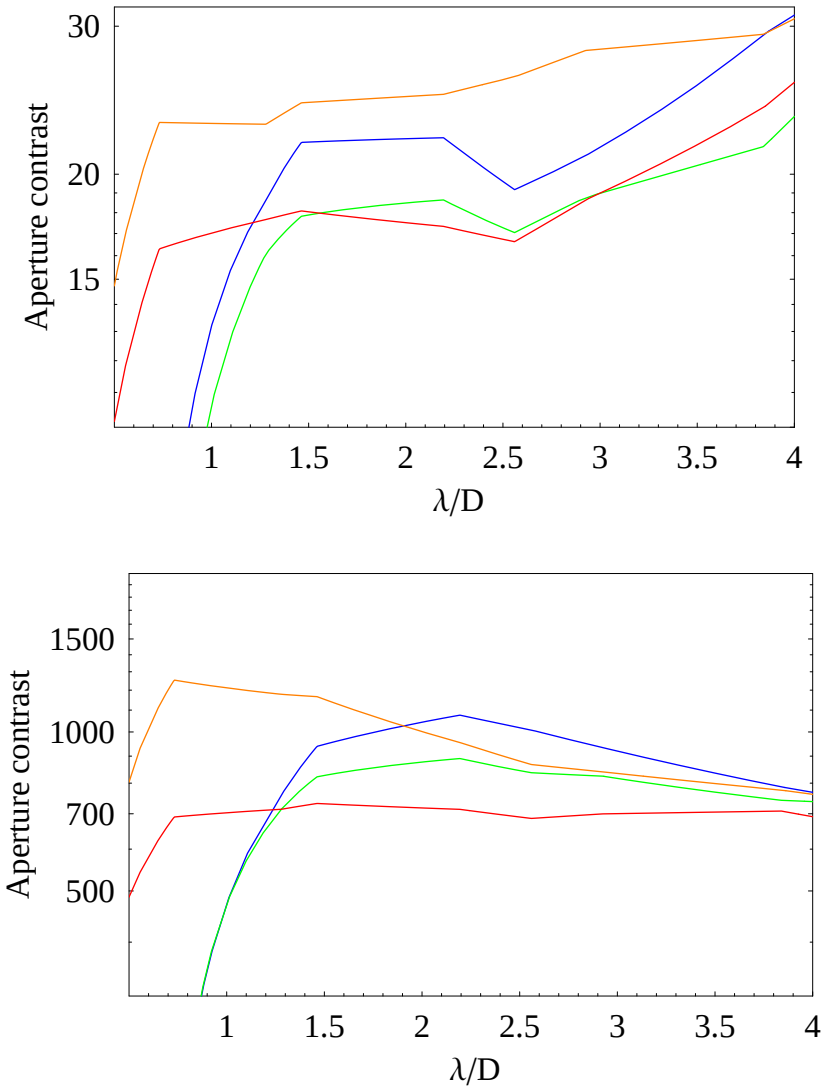

Figure 10: The attainable contrast through an aperture, as defined in the text. The analytical results would suggest that performance would converge (at least for the phase masks) at large radii and low turbulence, as observed in these results.

Figure 10 plots the dynamic range, defined as the flux through the aperture of an off-axis source, divided by the flux though this aperture from the off-axis source, as attenuated by the coronagraph. The general trends are as expected; all designs converge to a similar value at large radii, where performance is fixed by AO parameters. Inwards of this, as would be expected, the charge 6 design does somewhat better than charge 2 until a point is reached where the wider exclusion radius of the charge 6 mask attenuates the off-axis source markedly. These trends are rather similar for both levels of AO correction, although of course the attainable dynamic range is much better for a better-corrected wavefront. What is most apparent however is that the quadrant mask does better than the two pure vortex masks, and seems to have a well-balanced mixture of various charges to perform well at both large and small radii. The performance however will depend on angle relative to the phase discontinuities in the mask, which produce "blind lines". The prolate-apodized mask also performs well if the loss of light is not an issue.

A charge-2 OVC would be a good choice for an instrument which had no angular dependence of its response in the focal plane, but is more complex to manufacture than a quadrant phase mask. Whether there is an "optimum" mask of this type in some sense remains an open question.

3 Conclusions

The phase vortex mask is an interesting basis for a coronagraph because it offers the possibility of complete on-axis extinction of a pure Airy diffraction pattern. This result can be demonstrated analytically for even topological charges. Moreover, masks of even charges form the Fourier basis to build up many other varieties of phase mask, for example the quadrant mask, all of which will share the extinction property, and analytical tractability, of a single-charge mask. Odd charges always degrade performance so the class of useful masks is restricted by this fact.

A ground-based telescope however will typically have two aspects that degrade the performance of vortex phase masks, and phase masks derived from them. The central obstruction of the telescope, and the effects of atmospheric turbulence (even partially corrected) are limitations. "Removing" the central obstruction, by Guyon's method for example, seems essential to attain anything more than modest dynamic range, a conclusion which applies to either diffraction-limited images or moderate levels of AO correction.

This of course is a common problem for coronagraphs.

The effect of this class of phase masks can be analyzed quite generally when partially corrected turbulence is present, and the conclusion is that they will tend to remove the coherent core of the AO-corrected images and leave the incoherent power-law halo. The implied outer working radius is the "shoulder" in a typical AO image where the core meets the halo, largely independently of the details of the mask but fixed by details of the AO system such as the actuator density.

The inner working radius is however affected by the details of the mask. It is determined by the extinction of a hypothetical source adjacent to the on-axis one. Here the masks do differ, and it is possible to show that high-charge masks have a wider zone of extinction than low-charge ones. Taken together with the residual light that is transmitted from the on-axis source, the detailed simulations show that there is rather little to choose between the various masks considered here. In fact the quadrant mask is as good as any. High-charge masks seem to offer relatively small gains, for the particular turbulence parameters that were examined. The quadrant mask has the advantage of being relatively simple to manufacture[20], by comparison with a vortex where a smooth gradient in phase has to be achieved over the mask. Overall however the phase masks are not the limiting factor in dealing with AO imagery and it seems likely that a suitable mask could be designed for most applications by suitable tailoring of the basis set of vortex masks.

Appendix 1: Effect of the vortex filter on a partially-corrected image

In the Fourier optics approximation, as is well known, the mathematical description of a coronagraph requires three Fourier transforms. The first operates in the exit pupil of the telescope or adaptive optics system, and produces the amplitude distribution in the focal plane. This amplitude is modified by a stop or phase plate. A further (inverse) transform gives the resultant amplitude in a reimaged pupil plane, and here a Lyot or pupil stop is typically used to eliminate unwanted diffraction. A third transform is used to obtain the amplitude at a final focal plane. I will denote co-ordinates in the first pupil by r, the first focal plane by k, in the second pupil plane by r' and in the final focal plane by k'. A circular, unobstructed aperture is

assumed.

For a well-corrected adaptive optics system, the amplitude in the exit pupil is given by $\exp(\imath\phi(\vec{r})) \simeq 1 + \imath\phi(\vec{r})$. If the number of actuators is large (the mathematical requirement is that the scale of correlation of the phase is much shorter than the pupil size) the a standard argument gives the long-exposure point spread function (PSF). This is the diffraction-limited PSF of the pupil, scaled by the Strehl ratio, plus a halo which is proportional to the power spectrum of the phase, scaled by (1-Strehl). (The appearance of a second-order quantity, namely the power spectrum of the phase, indicates that for consistency the phase exponential has to be expanded to second order. Carry these second-order terms through the calculation gives the appropriate scalings of "core" and "halo" by phase variance or Strehl ratio.)

Subject to the same assumptions, it is possible to find the PSF in the final focal plane, after application of a vortex phase filter in the first focal plane, and a pupil stop in the reimaged pupil. For an unobstructed diffraction-limited system, the final PSF is of course zero; for partial correction, the PSF is just the phase power spectrum. The vortex filter removes the coherent component, the Airy disc, and only the incoherent part passes through.

I now give the details of this argument, which, although cumbersome, involves only the repeated application of the physical approximations already stated. For simplicity, constants of proportionality that are unnecessary to the main argument will be omitted.

In the first focal plane, the amplitude will be (proportional to is understood from here on) -

$$\mathcal{A}(\vec{k}) = \mathcal{A}(\vec{k}) + \imath \int d\vec{r}\, \phi(\vec{r}) \exp(\imath\vec{k} \cdot \vec{r})\Omega(\vec{r})$$

in which $\vec{k}$ denotes a (suitably scaled) position in the focal plane, A is the Airy amplitude pattern, and $\Omega(\vec{r})$ is a function which is unity inside the pupil and zero outside.

This amplitude is multiplied by a vortex filter function $f(\vec{k})$ which is of the form $\exp(\imath m\theta)$, m being an even integer and θ being the azimuthal angle in the focal plane. $ff^* = 1$ will be a useful property later in the argument.

Propagating to the reimaged focal plane, and applying the full-size pupil stop there gives an amplitude leaving that pupil which is

$$\Omega(\vec{r'}) \int d\vec{k}\, \mathcal{A}(\vec{k}) f(\vec{k}) \exp(-\imath\vec{k} \cdot \vec{r'}).$$

Here $\vec{r'}$ is the co-ordinate in the reimaged pupil. The extinction property of the even-charge vortex filter is that

$$\Omega(\vec{r'}) \int d\vec{k}\, A(\vec{k}) f(\vec{k}) \exp(-\imath \vec{k} \cdot \vec{r'}) = 0,$$

so the amplitude leaving the reimaged pupil is

$$\imath\Omega(\vec{r'}) \int d\vec{k}\, \left(\int d\vec{r}\, \phi(\vec{r}) \exp(\imath \vec{k} \cdot \vec{r}) \Omega(\vec{r}) \right) f(\vec{k}) \exp(-\imath \vec{k} \cdot \vec{r'}).$$

Finally, therefore, the amplitude in the second focal plane will be

$$\mathcal{A}'(\vec{k'}) = \int d\vec{r'}\, \imath\Omega(\vec{r'}) \int d\vec{k}\, \int d\vec{r}\, \phi(\vec{r}) \exp(\imath \vec{k} \cdot \vec{r}) \Omega(\vec{r}) f(\vec{k}) \exp(-\imath \vec{k} \cdot \vec{r'}) \exp(\imath \vec{k'} \cdot \vec{r'}).$$

The time- or ensemble-averaged intensity is

$$I(\vec{k'}) = \left\langle \mathcal{A}'(\vec{k'}) \mathcal{A}'^{*}(\vec{k'}) \right\rangle.$$

To carry out the sixfold integration and averaging, write

$$\begin{aligned} \mathcal{A}'^{*}(\vec{k'}) &= \int d\vec{r'_1}\, (-\imath)\Omega(\vec{r'_1}) \int d\vec{k}_1\, \int d\vec{r}_1\, \phi(\vec{r_1}) \exp(-\imath \vec{k_1} \cdot \vec{r_1}) \Omega(\vec{r_1}) f(\vec{k_1})^{*} \times \\ &\times \exp(\imath \vec{k_1} \cdot \vec{r'_1}) \exp(-\imath \vec{k'_1} \cdot \vec{r'_1}). \end{aligned}$$

in which the subscript 1 is used to indicate corresponding dummy variables of integration.

Re-arranging the order of integration, the first part of the sixfold integration involves $\vec{r}$ and $\vec{r_1}$:

$$\int \int d\vec{r}\, d\vec{r}_1\, \langle \phi(\vec{r}) \phi(\vec{r_1}) \rangle \exp\left(\imath \vec{k} \cdot \vec{r} - \imath \vec{k_1} \cdot \vec{r_1} \right) \Omega(\vec{r}) \Omega(\vec{r_1}).$$

Writing $\vec{r_1} = \vec{r} + \vec{u}$, the integral contains the term

$$\langle \phi(\vec{r}) \phi(\vec{r} + \vec{u}) \rangle \simeq \mathcal{C}(\vec{u})$$

which is approximately equal to the spatially-invariant phase autocorrelation function $\mathcal{C}$ (the equality cannot be exact because of the edges of the pupil). If $\mathcal{C}$ declines rapidly with $\vec{u}$ (many actuators), then the $\vec{u}$ and $\vec{r}$ integrals separate to give the approximate result for this first pair of integrals as

$$\mathcal{P}(\vec{k_1})A(\vec{k}-\vec{k_1})$$

in which P is the phase power spectrum. This will turn out to be all that passes through the vortex coronagraph.

The next pair of integrals is

$$\int\int d\vec{k}d\vec{k}_1 f(\vec{k})f(\vec{k_1})^* \exp\left(-\imath\vec{k}\cdot\vec{r'}+\imath\vec{k_1}\cdot\vec{r_1'}\right)\mathcal{P}(\vec{k_1})A(\vec{k}-\vec{k_1}).$$

The Airy amplitude A is strongly peaked compared to other terms, and picks out $\vec{k}=\vec{k_1}$. The phase function f has unit modulus and so disappears, leaving

$$\int d\vec{k}\exp\left(-\imath\vec{k}\cdot\vec{r'}+\imath\vec{k}\cdot\vec{r_1'}\right)\mathcal{P}(\vec{k}) = \mathcal{C}(\vec{r_1'}-\vec{r_1}).$$

The final pair of integrals is

$$\int\int d\vec{r}d\vec{r}_1 \exp\left(-\imath\vec{k'}\cdot\vec{r'}-\imath\vec{k'}\cdot\vec{r_1'}\right)\mathcal{C}(\vec{r_1'}-\vec{r_1})\Omega(\vec{r'})\Omega(\vec{r_1'}).$$

With the same change of variable, and the same argument about the scale of $\mathcal{C}$ compared to the pupil size, it follows that

$$I(\vec{k'}) \simeq P(\vec{k'})$$

so that the effect of the vortex filter is to remove the coherent Airy core of the PSF and leave only the incoherent halo.

Appendix 2: Analytical estimate of off-axis behaviour of a vortex

In the high-Strehl approximation the optical vortex filter acts mainly on the diffraction-limited core of the AO-corrected PSF. It is important to know what happens when this core is not centered on the vortex filter, as this will be the case for point sources of interest near to a bright star. In the high-Strehl limit, where the amplitude is linear in the residual phase, the filter will act on the off-centered Airy disc but pass the uncorrelated (halo) light, as is the case for an on-axis source. In this section I show that the

transmitted energy is a simple power-law function of the offset distance in the focal plane.

Let us therefore consider an Airy pattern, off-axis by an amount s at some angle α (with respect to the origin of the focal plane co-ordinate system (k, θ). To simplify the discussion, I work in scaled units of length in both the pupil plane and focal plane. In the pupil plane, scale lengths by the pupil radius, and in the focal plane, scale by the factor $F\lambda/\pi$, F being the focal ratio of the system and λ the operating wavelength. This means that the Fourier transforms and PSFs can be written compactly.

The functional form of the off-axis Airy pattern is the standard one in a variable κ, with

$$\kappa = \Big(k^2 + s^2 - 2ks\cos(\alpha - \theta)\Big)^{1/2}$$

k being the scaled radial co-ordinate in the focal plane system centered on the vortex filter. The Airy pattern is therefore given (to within constants irrelevant to this discussion) by $J_1(\kappa)/\kappa$.

To write this in the needed variables, namely k and s, I apply the Gegenbauer identity[21]. Applying this to the present case,

$$\frac{J_1(\kappa)}{\kappa} = 2\sum_{n=0}^{\infty}(1+n)\frac{J_{n+1}(s)}{s}\frac{J_{n+1}(k)}{k}C_n^1(\cos(\alpha-\theta)) \tag{4}$$

in which C_k^1 is a Gegenbauer polynomial[22].

To evaluate the transmission of an off-axis source through the centered vortex filter, we can perform a Fourier transform, term by term, of the amplitude after the vortex filter

$$\exp(\imath m\theta)\,\frac{J_1(\kappa)}{\kappa}$$

in which the transform is with respect to the variables k and θ, and carries the intensity into a re-imaged focal plane in which the co-ordinates are $\vec{r}$.

If the source is on axis, there is no amplitude within the re-imaged pupil $\Omega(\vec{r})$ - this is the coronagraphic behaviour of the vortex filter. Off-axis, we can find the leading order term in s for which there is a finite amplitude within Ω. This gives an estimate of the near-to-axis transmission behaviour of the vortex filter.

Off axis (non-zero s) is more complicated mathematically but involves no new physics. The steps are as follows.

(1) In the Fourier transform into the re-imaged pupil

$$\int d\vec{k}\, \exp \imath m\theta \, \frac{J_1(\kappa)}{\kappa} \, \exp\left(\imath \vec{k} \cdot \vec{r}\right)$$

we note that

$$\vec{k} \cdot \vec{r} = kr\cos(\beta - \theta)$$

in which the polar co-ordinates in the re-imaged pupil are r and β. The transform is therefore

$$\int k\, dk \int d\theta \, \exp(\imath m\theta) \, \frac{J_1(\kappa)}{\kappa} \, \exp\left(\imath kr\cos(\beta - \theta)\right)$$

(2) We then insert the Gegenbauer expansion for $J_1(\kappa)/\kappa$. Expanding the Gegenbauer polynomials, and using multiple-angle formulas, rather than powers, we find that the angular integral in the transform involves terms which are of the form

$$\int d\theta \, \exp\left(\imath m\theta\right) \exp\left(\imath kr\cos(\beta - \theta)\right) \cos(p(\alpha - \theta))$$

with m and p both integers. These integrals can be systematically evaluated by using the identity[23]

$$\exp\left(\frac{z}{2}\,(t - \frac{1}{t})\right) = \sum_{n=-\infty}^{\infty} t^n J_n(z), \tag{5}$$

with the substitution $t = \exp(\imath(\beta - \theta))$, followed by multiplication by the appropriate cosine factor and then term-by-term integration. The result involves terms in J_{p-m} and J_{p+m}, as well as trigonometrical factors in β.

(3) The purpose of this calculation is to evaluate the transmission of the coronagraph at small s, so at this stage we limit the Gegenbauer series by expanding the $J_{n+1}(s)/s$ term to third order in s. This limits the expansion to fourth order Bessel functions and a third order Gegenbauer polynomial.

(4) We now have the k-integral to do. This resolves into a number of integrals of the Weber-Schafheitlin type ([11], namely

$$\int_0^\infty \frac{J_\mu(at)J_\nu(bt)}{t^\lambda}\, dt$$

which have a discontinuity at $a = b$ and different behaviour at $a > b$ and $a < b$. In our case, this behaviour corresponds to whether any light is diffracted beyond the vortex filter into the re-imaged pupil.

(5) We carried out this lengthy series of calculations in the computer algebra package *MATHEMATICA*, and investigated topological charges on the vortex masks of $m = 2, 3, 4, 5, 6$. What is of interest is to note the first power of s, the focal-plane offset, that gives any diffracted light *within* the re-imaged pupil. If this power is γ then this means that the transmission energy of an off-centered image is proportional to $(s/s_0)^{2\gamma}$. For odd topological charges, light is diffracted into the pupil regardless of offset; this corresponds to the known result that these charges are ineffective in a coronagraph. For even charges, we find the interesting result that $2\gamma = m$, so that the exponent equals the charge. This means that high-charge vortex filters will have a much steeper response to off-axis objects.

(6) Finally, we evaluate s_0 by integrating the leading-order term in s over the re-imaged pupil. What is of interest here is the relative behaviour, so we evaluate with respect to the energy passed by a $m = 0$ filter. This takes care of the various multiplicative constants that have been ignored so far. In (focal plane) scaled variables, the transmission of energy I for charges 2, 4 and 6 is given by

$$\begin{aligned} I_2 &= \frac{s^2}{6} \\ I_4 &= \frac{s^4}{32} \\ I_6 &= \frac{s^6}{240} \end{aligned}$$

This result is illustrated in Figure 11

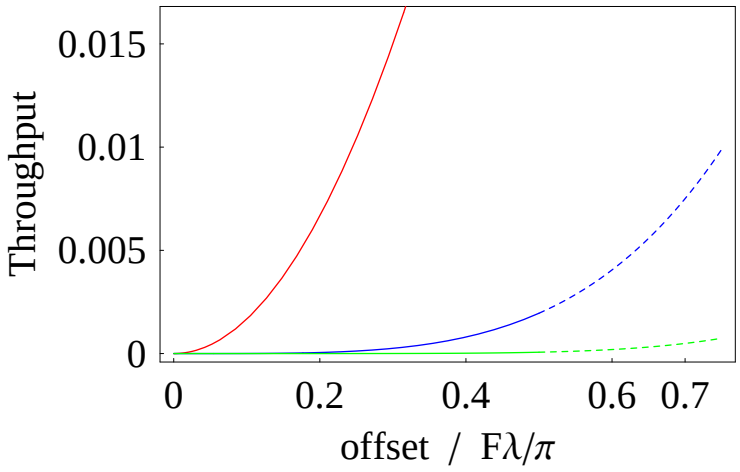

Figure 11: The transmitted intensity through a vortex, as a function of off-axis angle, for charges 2 (red), 4 (blue) and 6 (green). The analytical approximation only applies at small s and to emphasize this, lines are shown dashed beyond $s = 0.5$

Here is a specific example of the calculation for a charge 2 vortex. Expanding the Gegenbauer series (Equation 4) to third order in s gives

$$\begin{aligned}\frac{J_1(\kappa)}{\kappa} &= \frac{J_1(k)}{k} + \\ &+ s\left(\frac{J_2(k)\cos(\theta-\alpha)}{r}\right) + \\ &+ s^2\left(\frac{-3J_1(k)+3J_3(k)+6J_3(k)\cos(2\theta-2\alpha)}{24k}\right) + \\ &+ s^3\left(\frac{-2J_2(k)\cos(\theta-\alpha)+J_4(k)\cos(\theta-\alpha)+J_4(k)\cos(3\theta-3\alpha)}{24k}\right)\end{aligned}$$

The Fourier transform back into the pupil involves the term-by-term integration

$$\int k\,dk \int d\theta\, \exp(\imath 2\theta)\,\frac{J_1(\kappa)}{\kappa}\,\exp\left(\imath kr\cos(\beta-\theta)\right)$$

in which we specialize to the charge 2 case as an illustration. The variable r is the scaled co-ordinate in the re-imaged pupil plane.

The first term (no dependence on offset s) for the pupil-plane amplitude A is

$$\begin{aligned}A(r) &= 0 \qquad 0 \le r < 1 \\ &= \frac{-2\pi\exp(2\imath\beta)}{r^2} \quad r \ge 1.\end{aligned}$$

The next term (linear in s) is

$$\begin{aligned}A(r) &= \imath\pi s\exp(\imath(\alpha+\beta))\,r \qquad 0 \le r < 1 \\ &= \frac{-\imath\pi s\exp(-\imath(\alpha-3\beta))}{r^3} \quad r \ge 1.\end{aligned}$$

Here we see the first appearance of finite amplitude *within* the pupil. For larger charges the calculations have to be carried to higher in s before this happens. Figure 12 illustrates the appearance of the reimaged pupil, calculated in this analytical fashion, for a small offset of a source in the case of a charge 6 vortex.

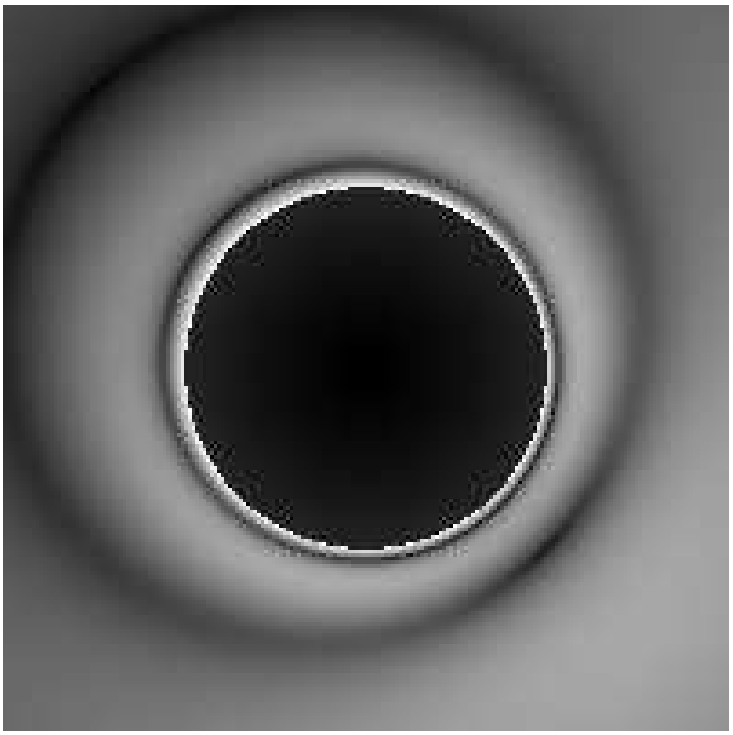

Figure 12: The transmitted intensity (stretched scale) in the pupil through a charge 6 vortex, for a small offset of the source in the focal plane. This was calculated analytically by the method in the text.

A useful check is to repeat this calculation for no vortex, namely a charge of zero. Although complicated expressions result, they simplify as expected; the intensity is uniform over the pupil, with a constant phase gradient.

Appendix 3. The quadrant mask as a superposition of vortex masks

The quadrant mask amplitude is defined as a function of azimuthal angle θ in the focal plane as

$$\begin{aligned}
\mathcal{A}(\theta) &= 1 \quad 0 \le \theta < \pi/2 \\
\mathcal{A}(\theta) &= -1 \quad \pi/2 \le \theta < \pi \\
\mathcal{A}(\theta) &= 1 \quad \pi \le \theta < 3\pi/2 \\
\mathcal{A}(\theta) &= -1 \quad 3\pi/2 \le \theta < 2\pi
\end{aligned}$$

with no radial dependence. This amplitude can be expressed as a Fourier series:

$$\mathcal{A}(\theta) = \frac{\pi}{2\imath}(\ldots + \frac{1}{5}e^{-10\imath\theta} + \frac{1}{3}e^{-6\imath\theta} + e^{-2\imath\theta} + e^{2\imath\theta} + \frac{1}{3}e^{6\imath\theta} + \frac{1}{5}e^{10\imath\theta} + \ldots) \quad (6)$$

so, a sum of various evenly charged vortex phase masks.

The effect of this (or other phase masks represented as Fourier series) can be analyzed analytically for an Airy diffraction pattern. Diffraction from the focal plane will involve integrals of the form

$$\int_0^\infty dr\, r\frac{J_1(k)}{k}\int_0^{2\pi} d\theta\, \mathcal{A}(\theta)\exp(\imath kr\cos(\theta-\beta))$$

which requires the result

$$\int_0^{2\pi} d\theta\, \exp(\imath n\theta)\exp(\imath z\cos(\theta-\beta)) = 2\pi\exp(\imath n\beta)J_n(z)$$

for z real and n an integer. (This can be deduced from Equation 5 by the method described there.)

The radial integrals are then of the Weber-Schafheitlin form, so the amplitude in the reimaged pupil is a weighted sum of the amplitudes for the various vortex masks that appear in Equation 6. Each of these is zero within the pupil as long as only evenly charged vortices appear in Equation 6.

As an example, Figure 13 shows a numerical and an analytical calculation of the reimaged pupil plane after application of a quadrant phase mask. This technique allows analytical calculations to be performed for any useful phase mask which does not have a radial dependence of the phase.

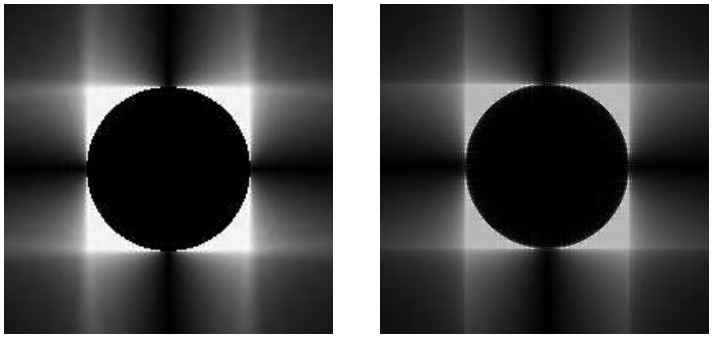

Figure 13: The transmitted intensity (stretched scale) in the pupil through a quadrant phase mask, calculated numerically (right) and analytically with ten non-zero terms in the Fourier expansion.

References

[1] O. Guyon, E. A. Pluzhnik, M. J. Kuchner, B. Collins, and S. T. Ridgway, "Theoretical Limits on Extrasolar Terrestrial Planet Detection with Coronagraphs," Astrophys. J. Suppl., **167,**, 81 (2006).

[2] G. Foo, D. M. Palacios and G. A. Swartzlander Jr., "Optical Vortex Coronagraph," Opt. Lett. **30**, 3308 (2005).

[3] J.H. Lee, G. Foo, E.G. Johnson, G. A. Swartzlander Jr., "Experimental Verification of an Optical Vortex Coronagraph," Phys. Rev. Lett., **97**, 053901 (2006).

[4] D. M.Palacios and G. A. Swartzlander Jr.,"The high-contrast performance of an optical vortex coronagraph", Proc. SPIE, **6288** 62880B (2006).

[5] O.Guyon, E. A.Pluzhnik M. J.Kuchner, B. Collins and S. T.Ridgway, "Theoretical Limits on Extrasolar Terrestrial Planet Detection with Coronagraphs," Astrophys. J. Suppl. Ser. **167**, 81 (2006).

[6] , G.A. Schwarzlander, Jr., "Achromatic optical vortex lens," Opt. Lett. **31**,2042 (2006).

[7] D. M.Palacios and S.L. Hunyadi, "Low-order aberration sensitivity of an optical vortex coronagraph," Opt. Lett. **31**, 2981 (2006).

[8] F. Roddier and C. Roddier, "Stellar Coronagraph with Phase Mask," Publ. Astr. Soc. Pac. **109**, 815 (1997).

[9] D. Rouan, P. Riaud, A. Boccaletti, Y. Clénet and A. Labeyrie, "The Four-Quadrant Phase-Mask Coronagraph. I. Principle," Pub Astr. Soc. Pac., **112**, 1479 (2000).

[10] D. Mawet, P. Riaud, O. Absil and J. Surdej, "Annular groove phase mask coronagraph," Astrophys. J. **633**, 1191 (2005).

[11] G.N. Watson, "A treatise on the theory of Bessel functions, 2nd edition," section 13.4. Cambridge University Press (1944).

[12] J. A. Dooley and P. R. Lawson,"Technology Plan for the Terrestrial Planet Finder Coronagraph," JPL Publication 05-8 (2005).

[13] M. Johns, R. Angel, S. Shectman, R. Bernstein, D. Fabricant, P. McCarthy, M. Phillips,"Status of the Giant Magellan Telescope (GMT) Project," Proc SPIE **5489**, 441 (2004).

[14] O. Guyon, "Phase-induced amplitude apodization of telescope pupils for extrasolar terrestrial planet imaging," Astron. Astrophys. **404**, 379 (2003).

[15] D. Gratadour, D. Rouan, A. Boccaletti1, P. Riaud and Y. Clnet,"Four quadrant phase mask K-band coronagraphy of NGC 1068 with NAOS-CONICA at VLT," Astron. Astrophys. **429**, 433 (2005).

[16] J.-L. Beuzit et al. A Planet Finder instrument for the VLT - in Direct Imaging of Exoplanets: Science & Techniques Proceedings IAU Colloquium No. 200

[17] B. Macintosh, J. Graham, D. Palmer, R. Doyon,D. Gavel, J. Larkin, B. Oppenheimer, L. Saddlemyer, J. K. Wallace, B. Bauman, J. Evans, D. Erikson, K. Morzinski, D. Phillion, L. Poyneer, A. Sivaramakrishnan, R. Soummer, S. Thibault and J.-P. Veran,"The Gemini Planet Imager," in Advances in Adaptive Optics II. SPIE, Volume 6272, pp. 62720L (2006).

[18] R Soummer, C Aime and P.E. Falloon, "Stellar coronagraphy with prolate apodized circular apertures", Astron. Astrophys. **397**, 1161, (2003).

[19] A. Sivaramakrishnan, C.D. Koresko, R.B. Makidon, T. Berkefeld, and M.J. Kuchner, "Ground-based Coronagraphy with High-order Adaptive Optics," Astrophys. J., **552**, 397 (2001).

[20] P. Riaud, A. Boccaletti, J. Baudrand, and D. Rouan, "The Four-Quadrant Phase Mask Coronagraph. III. Laboratory Performance", Pub. astr. Soc. Pac., **115**, 712 (2003).

[21] G.N. Watson, "A treatise on the theory of Bessel functions, 2nd edition," section 11.4. Cambridge University Press (1944).

[22] M. Abramowitz and I. A. Stegun, "Handbook of Mathematical Functions," Chapter 22, National Bureau of Standards (1964).

[23] G.N. Watson, "A treatise on the theory of Bessel functions, 2nd edition," section 2.1. Cambridge University Press (1944).